Miltefosine increases macrophage cholesterol efflux and inhibits NLRP3-inflammasome assembly and IL-1β release.

Iacano: Miltefosine inhibits macrophage IL-1β release

Amanda J Iacano[1], Harvey Lewis[1], Jennie E Hazen[1], Heather Andro[1], Jonathan D Smith[1,2*], and Kailash Gulshan[1*]

[1]Department of Cellular and Molecular Medicine, Cleveland Clinic, Cleveland OH 44195, USA.
[2]Department of Cardiovascular Medicine, Cleveland Clinic, Cleveland OH 44195, USA.

Total Word count: 7938
Word count of abstract: 197
Total characters with spaces: 55,063
Numbers of figures: 7

*****Correspondence to: Kailash Gulshan, Ph.D. or Jonathan D. Smith, Department of Cellular and Molecular Medicine, Cleveland Clinic, Cleveland OH , 9500 Euclid Avenue, Box NC10 Cleveland, OH 44195, Phone: 216-445-3699), Email: gulshak@ccf.org or smithj4@ccf.org.

Key Words: Cholesterol; ATP Binding Cassette Transporter A1; Autophagy; Inflammation

Abstract:

We tested Miltefosine, an FDA approved drug, for multiple effects in macrophages including cholesterol efflux, phospholipid trafficking, autophagy, and inflammation. Miltefosine increased ABCA1 mediated cholesterol efflux in RAW264.7 macrophages in absence of any cholesterol acceptor. Miltefosine increased lipid-raft disruption and cell surface phosphatidylserine (PS) exposure via decreased flip of PS from the cell-surface. Miltefosine treatment induced redistribution of phosphatidylinositol 4,5-bisphosphate from the plasma membrane to the actin rich regions in the cells. Miltefosine induced basal autophagy as indicated by increased p62 and LC3-II puncta formation. Free cholesterol levels were increased via degradation of lipid-droplets in Miltefosine treated cells. TLR4 signaling pathway was blunted by Miltefosine in mouse bone marrow derived macrophages, leading to ~75% reduction in pro-IL-1β mRNA levels. Miltefosine potently inhibited NLRP3 speck formation and the release of mature IL1-β. However, Miltefosine did not alter AIM2 inflammasome activity, indicating specific targeting of NLRP3 inflammasome pathway by Miltefosine. Endotoxin induced reactive oxygen species generation was significantly blunted by Miltefosine. Miltefosine pretreatment also prevented endotoxin mediated loss of mitochondrial membrane potential. Overall, Miltefosine targets multiple pathways in macrophages that are involved in atherosclerosis, inflammation, and metabolic diseases. The detailed investigation of mechanisms involved in Miltefosine's action may led to novel therapeutic targets for treating inflammatory disease such as atherosclerosis.

Non-standard abbreviations and acronyms:

ABCA1, ATP-binding cassette transporter A1
AIM2, absence in melanoma 2
AMPK, AMP-activated protein kinase
apoA1, apolipoprotein A-I
ASC1, apoptosis-associated speck protein containing a CARD (Caspase activation and recruitment domain)
Gsdmd; Gasdermin D
HDL-C, high-density lipoprotein-cholesterol
IL1-β, Interleukin 1-beta
LXR, liver X receptor
NLRP3, NOD-like receptor family pyrin domain-containing 3
NF-kB, nuclear factor kappa-light-chain-enhancer of activated B cells
PC, phosphatidylcholine

PIP2, phosphatidylinositol 4,5-bisphosphate
PS, phosphatidylserine
SR-BI, scavenger receptor-BI
TLR, toll like receptor

Significance Statement:

Atherosclerosis is driven by cholesterol accumulation and inflammation, and the arterial macrophage is a key cell type in both of these processes. The macrophage characteristics that protect against atherosclerosis include increased cholesterol efflux/reverse cholesterol transport, increased autophagy, and deceased inflammatory cytokine production and signaling. Here, we show that one single orally available compound, Miltefosine, can target multiple macrophage pathways involved in lipid homeostasis and inflammation. Miltefosine activated cholesterol efflux and autophagy while inhibited pro IL-1β gene expression and NLRP3 inflammasome assembly. In addition, Miltefosine reduced endotoxin-mediated mitochondrial reactive oxygen species and protected the mitochondrial membrane potential. The detailed investigation of mechanisms involved in Miltefosine's action may lead to novel therapeutic targets for preventing and treating atherosclerotic cardiovascular diseases.

Introduction:

Atherosclerosis, a sterile inflammatory disease, is the major cause of coronary artery disease (CAD). LDL cholesterol drives atherosclerosis by depositing LDL into the arterial intima, where it can be modified to induce endothelial cell activation and the recruitment of leukocytes; and, the uptake of modified LDL into macrophages leads to foam cell formation and a further amplification of inflammation [1 2]. Accumulation of oxidized lipids and cholesterol crystals in plaques activate toll-like receptor (TLR) pathways and the assembly of the NLRP3 inflammasome [3, 4]. The NLRP3 inflammasome is activated in aortas of advanced atherosclerosis patients as well as in other metabolic diseases such as obesity[5 6, 7]. The NLRP3 inflammasome plays a key role in processing procaspase 1 resulting in subsequent caspase 1 mediated processing of pro IL-1β to generate active interleukin-1β (IL-1β). The role of IL-1β in promoting human CAD was highlighted by the recently concluded CANTOS trial, showing that anti-IL-1β therapy met the primary endpoint, *a* reduction in a composite of heart attack, stroke and cardiovascular death [8]. The chronological activation of TLR (for production of IL-1β mRNA) and NLRP3 (for processing and release of IL-1β) in advanced atherosclerotic plaques can lead to amplification of immune responses and plaque instability.

In contrast to atherogenic pathways, the atheroprotective pathways such as autophagy and cholesterol efflux become increasingly dysfunctional in aging, advanced atherosclerotic plaques, and in animal models of atherosclerosis and diabetes [4, 9, 10]. During lipophagy, lipid droplets are engulfed by autophagosomes that then fuse with lysosomes where cholesterol esters are hydrolyzed to generate free cholesterol [9, 10]. Many lines of evidence have shown that inhibition of autophagy by pharmacological or genetic intervention is associated with increased atherosclerotic plaque burden[4, 9, 11]. Once the free cholesterol is generated by lipid-droplet autophagy it can be transported back to liver for excretion via reverse cholesterol

transport (RCT) [12-16]. The first step in RCT involves ABCA1-mediated cholesterol and phospholipid efflux to generate nascent HDL; however ABCA1 expression can also disrupt lipid-rafts and dampen TLR recruitment to cell membrane[17]. Thus, the simultaneous induction of athero-protective pathways, such as cholesterol efflux and autophagy, along with dampening of atherogenic pathways such as TLR signaling and NLRP3 inflammasome assembly, may serve as a potent therapeutic treatment for CAD patients. Here, we report that Miltefosine, an FDA approved drug for treating visceral and cutaneous leishmaniasis, promoted cholesterol efflux, disrupted lipid-rafts and TLR4 signaling, increased cell-surface phosphatidylserine (PS) exposure, induced phosphatidylinositol 4,5-bisphosphate (PIP2) trafficking from plasma membrane (PM) to the cell interior, induced basal autophagy, reduced lipopolysaccharide (LPS) induced mitochondrial reactive oxygen species (ROS) generation, and blunted NLRP3 inflammasome assembly and IL-1β release.

Results:

Miltefosine induced Abca1 mediated cholesterol efflux from cells

Previous study have shown that Miltefosine and other alkylphospholipids induced cholesterol efflux from the HepG2 cells[18]. We tested effect of Miltefosine treatment on ABCA1 mediated cholesterol efflux in RAW 264.7 macrophages. The control and ABCA1 expressing cells were incubated with different doses of Miltefosine for 4h and cholesterol efflux to serum-free media in the absence of apoA1, the usual acceptor, was determined. As shown in ***Fig. 1A***, Miltefosine treatment of control cells led to a dose dependent moderate but significant increase in cholesterol efflux to media with 7.5μM showing ~1 % increase ($n=4$, $p<0.001$ by ANOVA) and 10 μM showing ~2.8 % increase vs control cells ($n=4$, $p<0.0001$ by ANOVA). The ABCA1-expressing cells showed more robust cholesterol efflux to acceptor-free media in presence of

Miltefosine with 7.5μM showing ~5.28 % increase (n=4, $p<0.01$ by ANOVA) and 10 μM showing (~10.9 % increase vs control cells, n=4, $p<0.0001$ by ANOVA). Western blot analysis of the total and cell-surface ABCA1 showed no major differences in control vs. Miltefosine treated cells (***Fig. 1B***), indicating that Miltefosine induced increase in cholesterol efflux was not due to increased ABCA1 levels. We observed the Miltefosine induction of cholesterol efflux in two additional cell lines, HEK293 and BHK. In both cases, addition of Miltefosine induced basal, and markedly induced ABCA1-mediated cholesterol efflux to the acceptor-free media (***Fig. 1C, S1***). To test if the lipid flippase activity of ABCA1 is required for increased cholesterol efflux observed in Miltefosine treated cells, we used HEK293 cells stably expressing WT-ABCA1 isoform or a tangier disease mutant W590S-C1477R-ABCA1 isoform. The WT ABCA1 can flip phosphatidylserine (PS) and phosphatidylinositol 4,5-bisphopshate (PIP2) across plasma membrane[19]. The W590S mutation in ABCA1 decreased PS flip[20] while C1477R decreased PIP2 flip[19]. The HEK293 cells expressing WT and mutant isoform of ABCA1 were loaded with radiolabeled cholesterol and cholesterol efflux to media was determined in presence and absence of Miltefosine. As shown in ***Fig. 1D***, the W590S-C1477R double mutant isoform of ABCA1 showed significantly lower cholesterol efflux to media, indicating that lipid flippase activity of ABCA1 is required for Miltefosine induced cholesterol efflux to media. We also determined the effect of Miltefosine on generation of microparticles by cells. The media from RAW264.7 macrophages incubated with ± Miltefosine for 4h was collected and analyzed by ZetaView small particle tracking analyzer. The media from the cells treated with Miltefosine had significantly higher microparticles as compared to control cells (***Fig. S2***). These data indicated that Miltefosine may be remodeling the plasma membrane leading to increased cellular cholesterol efflux to media.

Miltefosine disrupts lipid rafts and increased PS exposure by inhibiting PS flip

Lipid rafts are comprised mainly of PC, cholesterol and sphingomyelin[21], and play a role in AKT and TLR signaling pathways. Disruption of lipid-rafts by ABCA1 is proposed to provide a free cholesterol pool for efflux and hamper TLR signaling via reduced recruitment of TLR2/4 to lipid-rafts[22 17, 23]. Previous studies have also shown that Miltefosine uses lipid-rafts as entry portals to cells[24] and can also act as an lipid-raft disrupting agent to inhibit human mast cell activation[25]. We determined the status of lipid-rafts in Miltefosine treated RAW264.7 macrophages by staining for the ganglioside GM1 using Alexa647-labeled cholera toxin B, followed by either fluorescent microscopy or flow cytometry. As shown in ***Fig. 2A*** cells treated with 7.5 μM Miltefosine for 16h displayed less GM1-CTB staining vs. control cells. The flow cytometry quantification of Alexa647-labeled cholera toxin B binding showed ~ 26% decrease in Miltefosine treated cells vs. control cells (n=3, $p<0.004$ by t-test, ***Fig. 2B***). We have previously shown that membrane remodeling resulting in lipid raft disruption can increase cell-surface PS and promote cholesterol extraction from the cell membrane[26]. A flow-cytometry based Annexin Cy5 binding assay was used to investigate if Miltefosine increased PS exposure at the cell-surface. Cells expressing ABCA1 were used as positive control, as PS cell-surface exposure is increased by ABCA1's PS flop activity[19, 20]. As shown in ***Fig. 2C***, Miltefosine treated cells showed ~24% increase in Annexin Cy5 binding vs. untreated cells (n=4, $p<0.005$ by ANOVA posttest). As expected, the cells expressing ABCA1 also showed increased Annexin Cy5 binding (~23% increase vs control cells, n=4, $p<0.05$ by ANOVA posttest). The Annexin Cy5 binding was further increased by Miltefosine treatment in ABCA1 expressing cells (~39% increase vs control cells with ANOVA, mean± SD, n=4, $p<0.0005$). These data indicated that Miltefosine increased cell-surface PS exposure independent of ABCA1 PS floppase activity. The increased levels of cell surface PS may be due to decreased rate of PS flipping (inward translocation). To qualitatively observe the PS flipping across

plasma membrane (PM) in control and Miltefosine treated cells, the fluorescent head-group labeled NBD-PS was used. RAW264.7 cells ± 7.5uM Miltefosine treatment for 16h, were incubated with exogenously added NBD-PS at final concentration of 25 μM. In control cells, majority of the exogenous NBD-PS moved to intracellular compartments over a 15 min incubation period at 37°C, while Miltefosine treated cells displayed more NBD-PS at PM and less inside the cells (***Fig. 2D***). To quantitatively measure flipping of NBD-PS, we used a previously described flow-cytometry based method using a membrane-impermeable NBD quenching reagent sodium dithionite[26]. RAW cells treated with ± 7.5uM Miltefosine for 16h were incubated with NBD-PS for 15 min at 37 °C, followed by addition of sodium dithionite to selected aliquots and flow cytometry analysis. The amount of NBD-PS flipped into the cells was calculated by measuring the % of NBD fluorescence resistant to quenching by sodium dithionite. As shown in ***Fig. 2E***, Miltefosine treated cells flipped significantly lower amounts of NBD-PS vs. control cells, ~44% vs. ~70% respectively ($n=4$, $p<0.0002$ by t-test). These data indicated that Miltefosine inhibited PS flip from the cell surface, resulting in increased PS exposure at the cell surface.

PIP2 is redistributed from plasma membrane upon Miltefosine treatment

Similar to PS, phosphatidylinositol 4, 5-bisphosphate (PIP2) is also sequestered in the inner leaflet of the plasma membrane. To determine the effect of Miltefosine on PIP2 trafficking and localization, RAW264.7 cells were stably transfected with a PIP2 reporter plasmid containing 2 copies of the pleckstrin homology domain from phospholipase Cδ fused to GFP (2X-PH-PLC-eGFP). These cells were treated with ± 7.5 μM Miltefosine for 16h and PIP2 reporter localization was determined by fluorescent microscopy. As shown in ***Fig. 3A***, control cells showed uniform localization of the PIP2 reporter at the plasma membrane while the cells

treated with Miltefosine showed an additional localization of the reporter in a specific actin rich region of the cytoplasm in both fixed and live cells (***Fig. 3B, C***).

Miltefosine induced basal and lipid-droplet autophagy

Autophagy plays a protective role in atherosclerosis[10] and becomes increasingly impaired in advanced human plaques[9]. Autophagy plays an important role in hydrolyzing macrophage cholesterol ester stored in lipid droplets to generate free cholesterol that can be effluxed from the cells[10]. Given that Miltefosine increased cholesterol efflux from the cells, we tested if Miltefosine induced autophagy. RAW 264.7 macrophages were treated with ± 7.5 μM Miltefosine for 16h and we observed that the Miltefosine treated cells showed multiple p62 puncta in cytoplasm, while control cells had evenly distributed weak cytoplasmic signal with almost no p62 puncta signal (***Fig. 4A,*** upper panel). Miltefosine treatment also increased lipidated form of LC3 puncta formation in macrophages transfected with LC3-GFP plasmid (***Fig. 4A*** lower panel). Next, we evaluated whether the LC3 puncta formation was due to increased autophagic initiation or due to decreased autophagic flux. Decreased or blocked autophagy flux can also lead to accumulation of autophagic markers. If Western blot analysis shows increased LC3-II after chloroquine (an autophagy flux inhibitor) treatment, then autophagic flux is occurring. We found that the LC3-II protein levels were increased by 4.3-fold in Miltefosine treatment alone vs. control cells (***Fig.4B, 4C***), while there was an additional 3.1 fold increase in LC3-II protein levels with Miltefosine + chloroquine treatment compared to cells treated with Miltefosine alone. These data indicate that Miltefosine increased autophagic flux. Next, we tested effect of Miltefosine on generation of free cholesterol from cholesterol ester rich lipid droplets. RAW264.7 macrophages were loaded with 100 µg/ml acetylated LDL (AcLDL) for 24h followed by treatment with ± 7.5 µM Miltefosine and ± acyl-co A cholesterol O-acyltransferase (ACAT) inhibitor (ACATi) for 4h to prevent cholesterol re-esterification. The

total and free cholesterol levels were determined by enzymatic assay described previously[27]. As expected, the AcLDL loaded cells had a higher ratio of cholesterol ester to free cholesterol (***Fig. 4D***). The cells treated with ACATi had higher free cholesterol levels and thus lower CE:FC ratio, while the Miltefosine treated cells showed further lowering of CE:FC ratio, indicating increased levels of free cholesterol. We also tested the effect of Miltefosine on lipid-droplet degradation by loading RAW264.7 cells with 100μg/ml AcLDL for 24h, followed by treatment with ± Miltefosine for 4h and staining with Nile-red dye. Cells treated with Miltefosine showed reduced Nile-red staining as compared to control cells (***Fig. S3***). To quantify the lipid-droplets, cells loaded with AcLDL were treated with ± Miltefosine and ± AcatI for 4h at 37ºC and subjected to flow-cytometry analysis. A shown in ***Fig. 4E***, the cells chased with Miltefosine showed significantly reduced Nile-red staining as compared to control cells. Addition of AcatI to block regeneration of lipid-droplets from free cholesterol led to further decrease in Nile-red staining in Miltefosine treated cells. These data indicated that Miltefosine can induce lipid-droplet turnover. To gain insight into the mechanism by which Miltefosine induced autophagy in macrophages, we determined the phosphorylation status of AMPK in control vs Miltefosine treated RAW264.7 macrophages and found that the levels of phospho-AMPK were higher in Miltefosine treated macrophages (***Fig S4***).

Miltefosine decreased LPS mediated induction in IL-1β levels

We demonstrated in Fig 2A that Miltefosine reduces lipid-rafts, which play an essential role in TLR2/4 signaling pathway and atherosclerosis progression[17, 23, 28-30]. We tested if LPS mediated induction in de novo synthesis of pro IL-1β messenger RNA was affected by Miltefosine. Bone-marrow derived macrophages (BMDMs) ± Miltefosine pretreatment were incubated with 1μg/ml LPS for 4h, followed by qRT-PCR assay using IL-1β specific primers and control Actb (β-actin) primers. The LPS induced increase in levels of IL-1β levels were

markedly reduced in Miltefosine treated cells showing ~4.5 fold decrease (n=3, p<0.034 with two tailed t-test) (***Fig. 5A***). Next, we performed western blot analysis of protein levels of pro IL1-β in control vs. Miltefosine treated cells. A shown in ***Fig. 5B***, the LPS mediated induction in pro IL1-β protein levels was decreased in Miltefosine treated cells (~55% decrease). Taken together, these data indicated that Miltefosine disrupted lipid-rafts, dampened TLR signaling pathway and decreased the LPS mediated induction in IL-1β mRNA and protein levels in macrophages.

Miltefosine inhibited NLRP3 inflammasome assembly and IL-1β release: Cholesterol crystals can cause disrupt autophagolysosome membrane, leading to NLRP3 inflammasome assembly[3, 31]. We tested effects of Miltefosine treatment on inflammasome assembly and IL-1β release in bone-marrow derived macrophages. Control and BMDMs pretreated with 5 μM Miltefosine for 16h, were primed with LPS for 4h and incubated with ATP for 20 min, followed by probing with anti-ASC1 antibody for visualization of Nlrp3 inflammasome assembly (***Fig.6A S5, S6)***. BMDMs treated with LPS and ATP formed ASC specks in 41% cells (n=308 cells analyzed) while in BMDMs pretreated with Miltefosine only 12% of cells showed ASC specks (523 cells analyzed, p<0.0001 by two-tailed Fisher's exact test). Miltefosine treatment led to ~80% decrease in release of mature IL-1β to media as compared to control macrophages (two tailed t-test, mean± SD, n=3, p<0.0039) (***Fig.6B***). To decipher the mechanism by which Miltefosine inhibited Nlrp3 inflammasome assembly, we determined the mRNA and protein levels of various Nlrp3 inflammasome complex members in BMDMs with or without LPS priming. Miltefosine with LPS actually slightly increased the mRNA levels, beyond the effects of LPS alone, for Nlrp3, procaspase 1 and Gsdmd (***Fig. 6C***). In agreement with earlier published studies[32], western blot analysis showed robust induction in protein levels of NLRP3 upon LPS treatment, which was not reduced by Miltefosine treatment (***Fig. S7)***. Miltefosine did

not appreciably alter the protein levels of ASC or procaspase 1 ***(Fig. S7)***. The release of mature IL-1β from cells is regulated by Gasdermin D mediated pore formation on plasma membrane[33, 34]. We tested and found no alteration in Gasdermin D protein levels by Miltefosine treatment (***Fig. S7***). To test if Miltefosine specifically inhibited NLRP3 inflammasome assembly and IL-1β release, we determined the effects of Miltefosine on AIM2 inflammasome. The control and Miltefosine treated macrophages were primed with LPS (1mg/ml) for 4hrs followed by lipofectamine mediated transfection of poly (dA:dT) for 3 h. The media was collected and subjected to IL-1β ELISA and as shown in ***Fig. 6D***, there was no difference in levels of AIM2 induced IL-1β released from cells ± Miltefosine treatment (n=3, n.s. with ANOVA); thus, Miltefosine did not alter AIM2 inflammasome activity. Previous studies have shown that deficiency of abca1/abcg1 increases inflammation in macrophages and ABCA1 mediated cholesterol efflux in dendritic cells dampen inflammasome assembly [35, 36]. Though, we used unloaded BMDMs for these studies, there is a possibility that Miltefosine was inhibiting Nlrp3 inflammasome assembly via cholesterol depletion. To directly test the role of cholesterol depletion on Nlrp3 inflammasome assembly, we treated BMDMs with 5μM Miltefosine for 16h or with 1mM cyclodextrin for 45 minutes at 37°C, followed by LPS/ATP incubation. Although cholesterol levels in BMDMs treated with cyclodextrin were significantly lower as compared to Miltefosine treated cells (n=3, $p<0.01$ with ANOVA, ***Fig. 6E***), Miltefosine was much more effective than cyclodextrin in inhibiting inflammasome activity as assayed by IL-1β release (***Fig. 6F)*** and ASC specks formation (***Fig. S8***). Thus, Nlrp3 inflammasome inhibition by Miltefosine cannot be attributed solely to cholesterol depletion.

Miltefosine blocked Nlrp3 inflammasome in a cholesterol independent manner and reduced mitochondrial ROS production

Since Miltefosine treatment did not reduce the expression levels of Nlrp3 inflammasome pathway components such as Nlrp3, Asc1, Caspase 1 or Gasdermin D, we tested if Miltefosine affected mitochondrial reactive oxygen species (ROS) generation. Mitochondrial ROS drives NLRP3 inflammasome assembly[37] and mitochondrial cardiolipin provides a docking site for Nlrp3 protein binding and inflammasome assembly[38]. As shown in ***Fig. 7A***, LPS treatment induced ROS production in control BMDMs as evident by increased staining with MitoSox Red while the Miltefosine pretreated cells showed decreased MitoSox staining upon LPS treatment. To quantify the MitoSox signal, we performed flow-cytometry and found that Miltefosine treated cells showed a significant 43% reduction in LPS-induced MitoSox staining (***Fig. 7B).*** Next, we tested effect of Miltefosine treatment on mitochondrial membrane potential. The control and Miltefosine pretreated BMDMs were incubated with ± LPS for 1h and stained with TMRM for 30 min at 37°C, followed by fluorescent microscopy of live cells. The cells treated with LPS showed marked reduction in TMRM staining while cells pretreated with Miltefosine showed lower reduction in TMRM signal (***Fig. S9***). To quantify the TMRM signal, we performed flow-cytometry and found that LPS treated cells showed a significant 41% reduction in TMRM staining signal while cells pretreated with Miltefosine showed only 24 % reduction in TMRM staining signal upon LPS treatment (***Fig. 7C)***. Given that Miltefosine induced autophagy in macrophages, we tested role of Miltefosine in removing damaged mitochondria from via Mitophagy. Using mitophagy detection kit (Dojindo# MD01), live RAW 264.7 macrophages were loaded with 500 nM mitophagy dye for 30 min at 37°C, followed by treatment with ± Miltefosine for 4h and visualization of cells under fluorescent microscope. The control cells showed weak fluorescence while cells treated with Miltefosine showed bright fluorescence (***Fig. S10)***. To determine if the mitochondria is indeed fused to lysosomes, the lyso-dye (0.25 μM) was added to cells and cells were visualized under fluorescent microscopy. As compared

to control cells, the cells treated with Miltefosine showed markedly increased co-localization of mitophagy dye with lyso-dye indicating increased mitophagy (***Fig. 7D***). Thus, Miltefosine may inhibit inflammasome assembly by decreasing mitochondria ROS, preventing LPS mediated damage to mitochondria and by removing damaged mitochondria through mitophagy.

Discussion

Miltefosine is on the World Health Organization list of essential medicines and is FDA approved for treating cutaneous and visceral leishmaniasis. The structure of Miltefosine is similar to lyso-PC and it is known to integrate in the cell membrane and redistribute in intracellular membranes of ER, Golgi and mitochondria[39]. It is widely believed that most of the downstream effects of Miltefosine are dependent on cell-type, with range of activities such as induction of apoptosis in cancer cells and inhibition of Mast cell activation[25, 40]. However, the mechanism of action of Miltefosine, whether regarding killing of parasites or cancer cells, is not fully understood.

We found that Miltefosine has multiple activities in macrophages; induction in Abca1 mediated cholesterol efflux from cells to media, lipid-raft disruption, inhibition of PS flip from the outer to the inner leaflet of the plasma membrane, redistribution of plasma membrane PIP2 to cytoplasmic actin-rich regions, induction of basal autophagy, increased lipid droplet degradation, and inhibition of NLRP3 inflammasome assembly and IL-1β release. As shown before in HepG2 cells[18], Miltefosine increased both basal and ABCA1-induced cholesterol efflux from RAW264.7 murine macrophages in the absence of a cholesterol acceptor. Efflux in the absence of an acceptor can be due to microparticle generation that is increased by ABCA1[41], and Miltefosine effects on the plasma membrane may alter membrane fluidity and microparticle generation. The Miltefosine mediated increased cholesterol efflux activity of ABCA1 requires functional lipid flippase activity. The ABCA1 mutant isoform defective in PS

and PIP2 flippase activity showed lower cholesterol efflux to media in presence of Miltefosine as compared to WT-ABCA1 isoform. In addition, the Miltefosine mediated disruption of lipid-rafts can lead to a redistribution of plasma membrane free cholesterol and play a role in increased cellular cholesterol efflux.

Autophagy plays a protective role in atherosclerosis[10] and it is impaired in advanced human plaques[9]. Autophagy is controlled by multiple pathways responding to stimuli such as the status of cellular energy (AMP-dependent protein kinase, AMPK) or amino acid availability (target of rapamycin, TOR). Miltefosine induced basal autophagy in macrophages as evident by increased cytoplasmic p62 and LC3-GFP puncta. We showed that Miltefosine treatment increased the turnover of cholesterol esters in cholesterol loaded cells, supporting the notion that Miltefosine increased degradation of lipid-droplets via lipophagy. The increased phosphorylation of AMPK due to Miltefosine may lead to induced basal autophagy that we observed in Miltefosine treated cells. Add more here. AMPK is a key regulator of lipid and energy metabolism. AMPK plays a role in activating autophagy and is also implicated in aging. Decreased AMPK activity due to aging or inflammation can promote metabolic disorders such as cardiovascular disease and diabetes. Previous studies have shown that AMPK activation can prevent vascular damage cause by modified LDL and reduce insulin resistance.

Lipid-rafts play an essential role in recruiting TLRs to plasma membrane to initiate a signaling cascade that allows cytoplasmic NF-kB to shuttle inside the nucleus and upregulate pro IL-1β mRNA. Resting macrophages express low levels of pro IL-1β but macrophages primed with LPS induce the levels of pro IL-1β as well as NLRP3. Miltefosine treated cells had reduced induction of pro IL-1β transcript levels by LPS treatment. However, NLRP3 mRNA levels after LPS induction were similar in Miltefosine treated and control cells. Since both IL-1β and NLRP3 transcripts are induced by NF-kB, the different response to NF-kB may in part be

explained by the degree of induction, as the levels of NLRP3 transcripts were modestly increased (3-fold) compared to the robust (30,000- fold) induction of pro IL-1β transcript levels. Given the sharp decrease in levels of pro IL-1β transcript levels, in addition to a decrease in its synthesis, Miltefosine treatment may also lead to increased degradation of IL-1β transcripts.

The components of the inflammasome complex, NLRP3, ASC1, and Caspase1 are significantly increased in atherosclerotic plaques compared to healthy arteries. Blocking of NLRP3 by a chemical drug MCC9550 reduces atherosclerosis in mouse and infarct size in pigs [42, 43]; and, a recent trial showed reduced cardiovascular events in subjects treated with an anti IL-1β monoclonal antibody [8]. The protein levels of NLRP3 are not only controlled transcriptionally, but also by a non-transcriptional priming pathway involving TLR4 and Myd88 via NLRP3 deubiquitination[32]. Although Miltefosine inhibited NLRP3 inflammasome assembly, surprisingly, the levels of NLRP3 inflammasome components (ASC1, NLRP3, and Caspase 1) in resting as well as in LPS induced macrophages were unaltered in control vs. Miltefosine treated cells. Mature IL-1β is released via cleaved Gasdermin D pores[44], but Miltefosine treatment did not alter the levels of full length Gasdermin D, thus ruling out decreased Gasdermin D as a mechanism for Miltefosine. The intriguing question raised by these data is that if all inflammasome components are present and more or less equally induced by LPS in control vs. Miltefosine treated macrophages, why is the Nlrp3 inflammasome not assembled in Miltefosine treated cells. Recently it was shown that NLRP3 is localized to the trans golgi network via binding to PI4P prior to inflammasome assembly[45]. Miltefosine may work at this or other steps to block inflammasome assembly. Mitochondria also play an essential role in assembly of the Nlrp3 inflammasome[37, 46]. Miltefosine treated cells showed reduced levels of ROS upon LPS treatment (***Fig. 7E, F***). Based on our data, we speculate that Miltefosine treated macrophages failed to assemble Nlrp3 inflammasome due to lower levels of oxidative

stress and efficient removal of damaged mitochondria (mitophagy), thus blocking Nlrp3 inflammasome assembly

Given the effects of Miltefosine on NLRP3 inflammasome pathway and IL-1β release, it may serve as potential therapeutic for metabolic diseases where Nlrp3 inflammasome is hyper activated; such as diabetes, non-alcoholic fatty liver disease (NAFLD) and high fat diet induced inflammation. Miltefosine promotes cholesterol efflux from cells and thus can be used as adjuvant along with Statins. Miltefosine mediated cellular cholesterol depletion can lead to upregulation of cholesterol biosynthetic pathway, thus long-term Miltefosine treatment can be combined with drugs blocking cholesterol biosynthesis. Induction of autophagy and inhibition of Nlrp3 inflammasome by Miltefosine can also play a role in reduction of lipid burden and dampening of IL-1β pathway. Miltefosine can serve as anti-atherosclerotic and anti-inflammatory therapy for treatment and prevention of atherosclerosis and other metabolic diseases. Further work is required to fully understand the underlying molecular mechanisms responsible for spectrum of Miltefosine' s actions on macrophage cellular functions.

Material and Methods

A detailed description of the materials and methods used in this study is provided in *SI Materials and Methods*. Basic methods are summarized below.

Cell culture and reagents: All cell culture incubations were performed at 37ºC, unless otherwise indicated, in a humidified 5% CO_2 incubator. The growth media was Dulbecco's Modified Eagle Medium (DMEM) with 10% fetal calf serum, 100 µg/mL penicillin, 100 µg/mL streptomycin. Drugs were added to growth media at indicated concentrations and an equivalent amount of vehicle was added as control. Mifepristone ABCA1-inducible BHK cells, as previously described were obtained from Chongren Tang, University of Washington[47].

ABCA1-GFP and the mutant isoform stably transfected HEK cells were previously described[48]. Other materials are described in *SI Materials and Methods*.

Isolation of Bone marrow derived macrophages: Mice were maintained on chow diet and sacrificed at 16 weeks of age. Femurs were collected to isolate and culture bone marrow macrophages using conditioned L-cell media. Other details are described in *SI Materials and Methods*.

Isolation of total RNA from BMDM cell pellets and RT-PCR analysis: Total RNA was isolated from cell pellets using the RNeasy Mini Kit (Qiagen, Valencia, CA), following the manufacturer's protocol. On-column digestion with RNase-free DNase (Qiagen, Valencia, CA) was performed to remove genomic DNA. The qRT-pCR assays were performed using TaqMan reagent from ThermoFisher following the manufacturer's protocol. Other materials and details are described in *SI Materials and Methods*.

Cholesterol efflux assay: The cholesterol efflux assays were performed in HEK293-Abca1-GFP cells, BHK cells, or RAW 264.7 murine macrophages as described earlier[19]. Other details are described in *SI Materials and Methods*.

Lipid-Raft quantification: The lipid-raft were visualized under fluorescent microscope and quantified using flow-cytometry assay as described before[26]. Other details are described in *SI Materials and Methods*.

Mitochondrial ROS production and membrane potential measurement: For determining the mitochondrial ROS levels, control or Miltefosine treated BMDMs were primed with 1ug/ml LPS for 4h, followed by staining with Mitosox using manufacturer’s protocol. Cells were either visualized under fluorescent microscope or subjected to flow-cytometry analysis. For mitochondrial potential measurement, control or Miltefosine treated BMDMs were primed with

1ug/ml LPS for 4h, followed by staining with TMRM using manufacturer's protocol. Cells were either visualized under fluorescent microscope or subjected to flow-cytometry analysis.

Total/FC measurements: RAW264.7 cells grown in 12-well plates were loaded with 50 µg/ml cholesterol-CD or with 100 µg/ml AcLDL for 16 h at 37 °C with or without 2 µg/ml ACATi treatment for 2h. The total cholesterol and free cholesterol levels were determined by using enzymatic assay as described earlier[27].

Cell-surface PS and NBD-PS translocation: The flow cytometry based assays to determine cell-surface PS and translocation of NBD-PS were described earlier[26]. Other details are described in *SI Materials and Methods*.

Western blotting: RAW264.7 cells or BMDMs were grown treated as indicated. The PBS-washed cell pellet was lysed in NP40 lysis or MPER lysis buffer. After discarding the nuclear pellet, the protein concentration was determined using the BCA protein assay (Pierce). 10-50 µg of cell protein samples were resolved on SDS gel, followed by probing with primary and secondary horseradish peroxidase-conjugated antibodies. Total and cell-surface ABCA1 levels were determined as described earlier[26]. Other details are described in *SI Materials and Methods*.

Indirect immunofluorescence/fluorescent microscopy: RAW264.7 cells or BMDMs were grown in 4-chamber slides in indicated growth media. Cells were washed with 1xPBS, fixed with paraformaldehyde, and then incubated with permeabilization solution (1xPBS/0.2% Triton X-100) for 10 min at RT. Cells were washed with 1xPBS three times and blocked with normal goat serum (1xPBS/1%BSA/5% normal goat serum) at 37ºC for 30 min. The cells were probed with p62 antibody and Alexa 647 labeled secondary antibody. For LC3 staining, RAW264.7 cells were transfected with LC3-GFP (Addgene) using lipofectamine LTX according to manufacturer protocol (Life Technologies). Cells were treated with or without 7.5 µM

Miltefosine for 16 h. For ASC1 staining, Bone marrow derived macrophages from WT C57BL6 or C57BL6 apoE$^{-/-}$ KO mice were treated ± 5 μM Miltefosine for 16 h or ± 1mM cyclodextrin for 2h. Cells were washed with 1xPBS and fixed with 100% ethanol, followed by staining with anti-ASC antibody and Alexa 568 labeled secondary antibody. All images were captured using an Olympus IX51 inverted epifluorescent microscope, Olympus LUCPlanFl ×40/0.6 lens, with a Q-Image EXi aqua camera and Olympus cellSens Dimension version 1.7 software. Post-imaging processing was performed in Adobe Photoshop CS2.

PIP2 cellular reporter assay: RAW264.7 macrophage cell lines stably transfected with 2PH-PLCδ-GFP plasmid was described earlier[19]. Live or fixed cells were visualized by epifluorescent microscopy. All images were captured using an Olympus IX51 inverted epifluorescent microscope.

Statistical analyses: Data are shown as mean ± SD. Comparisons of 2 groups were performed by a 2-tailed t test, and comparisons of 3 or more groups were performed by ANOVA with Bonferroni posttest. All statistics were performed using Prism software (GraphPad).

Author Contributions

A.J.I., and H.L. performed the experiments. J.H. performed the PS translocation assay. J.D.S. provided help with data analysis. K. G. conceived of the project idea, designed and directed study, performed experiments, performed data analyses and drafted the manuscript. All authors critically reviewed the manuscript.

Acknowledgments

This research was supported by American Heart Association scientist development grant SDG25710128 to K.G and NIH grants R01 HL128268 and R01 HL130085 to J.D.S.

References

1. Moore, K.J. & Tabas, I. Macrophages in the pathogenesis of atherosclerosis. *Cell* **145**, 341-355 (2011).
2. Tabas, I. Macrophage death and defective inflammation resolution in atherosclerosis. *Nat Rev Immunol* **10**, 36-46 (2010).
3. Duewell, P. *et al.* NLRP3 inflammasomes are required for atherogenesis and activated by cholesterol crystals. *Nature* **464**, 1357-1361 (2010).
4. Razani, B. *et al.* Autophagy links inflammasomes to atherosclerotic progression. *Cell metabolism* **15**, 534-544 (2012).
5. Hansson, G.K. & Klareskog, L. Pulling down the plug on atherosclerosis: cooling down the inflammasome. *Nature medicine* **17**, 790-791 (2011).
6. Zheng, F., Xing, S., Gong, Z. & Xing, Q. NLRP3 inflammasomes show high expression in aorta of patients with atherosclerosis. *Heart Lung Circ* **22**, 746-750 (2013).
7. Stienstra, R. *et al.* Inflammasome is a central player in the induction of obesity and insulin resistance. *Proceedings of the National Academy of Sciences of the United States of America* **108**, 15324-15329 (2011).
8. Ridker, P.M. *et al.* Antiinflammatory Therapy with Canakinumab for Atherosclerotic Disease. *The New England journal of medicine* **377**, 1119-1131 (2017).
9. Liao, X. *et al.* Macrophage autophagy plays a protective role in advanced atherosclerosis. *Cell metabolism* **15**, 545-553 (2012).
10. Ouimet, M. *et al.* Autophagy regulates cholesterol efflux from macrophage foam cells via lysosomal acid lipase. *Cell metabolism* **13**, 655-667 (2011).
11. Sergin, I. & Razani, B. Self-eating in the plaque: what macrophage autophagy reveals about atherosclerosis. *Trends in endocrinology and metabolism: TEM* **25**, 225-234 (2014).
12. Khera, A.V. *et al.* Cholesterol efflux capacity, high-density lipoprotein function, and atherosclerosis. *The New England journal of medicine* **364**, 127-135 (2011).
13. Wang, X. *et al.* Macrophage ABCA1 and ABCG1, but not SR-BI, promote macrophage reverse cholesterol transport in vivo. *The Journal of clinical investigation* **117**, 2216-2224 (2007).
14. Yvan-Charvet, L., Wang, N. & Tall, A.R. Role of HDL, ABCA1, and ABCG1 transporters in cholesterol efflux and immune responses. *Arteriosclerosis, thrombosis, and vascular biology* **30**, 139-143 (2010).
15. Oram, J.F. ABCA1 as a New Therapeutic Target for Treating Cardiovascular Disease. *Drug news & perspectives* **15**, 24-28 (2002).
16. Oram, J.F. HDL apolipoproteins and ABCA1: partners in the removal of excess cellular cholesterol. *Arteriosclerosis, thrombosis, and vascular biology* **23**, 720-727 (2003).
17. Zhu, X. *et al.* Macrophage ABCA1 reduces MyD88-dependent Toll-like receptor trafficking to lipid rafts by reduction of lipid raft cholesterol. *Journal of lipid research* **51**, 3196-3206 (2010).
18. Rios-Marco, P., Jimenez-Lopez, J.M., Marco, C., Segovia, J.L. & Carrasco, M.P. Antitumoral alkylphospholipids induce cholesterol efflux from the plasma membrane in HepG2 cells. *J Pharmacol Exp Ther* **336**, 866-873 (2011).
19. Gulshan, K. *et al.* PI(4,5)P2 Is Translocated by ABCA1 to the Cell Surface Where It Mediates Apolipoprotein A1 Binding and Nascent HDL Assembly. *Circulation research* **119**, 827-838 (2016).
20. Alder-Baerens, N. *et al.* Headgroup-specific exposure of phospholipids in ABCA1-expressing cells. *The Journal of biological chemistry* **280**, 26321-26329 (2005).

21. Simons, K. & Toomre, D. Lipid rafts and signal transduction. *Nature reviews. Molecular cell biology* **1**, 31-39 (2000).
22. Landry, Y.D. *et al.* ATP-binding cassette transporter A1 expression disrupts raft membrane microdomains through its ATPase-related functions. *The Journal of biological chemistry* **281**, 36091-36101 (2006).
23. Yvan-Charvet, L. *et al.* Increased inflammatory gene expression in ABC transporter-deficient macrophages: free cholesterol accumulation, increased signaling via toll-like receptors, and neutrophil infiltration of atherosclerotic lesions. *Circulation* **118**, 1837-1847 (2008).
24. van der Luit, A.H. *et al.* A new class of anticancer alkylphospholipids uses lipid rafts as membrane gateways to induce apoptosis in lymphoma cells. *Mol Cancer Ther* **6**, 2337-2345 (2007).
25. Weller, K. *et al.* Miltefosine inhibits human mast cell activation and mediator release both in vitro and in vivo. *J Invest Dermatol* **129**, 496-498 (2009).
26. Gulshan, K., Brubaker, G., Wang, S., Hazen, S.L. & Smith, J.D. Sphingomyelin Depletion Impairs Anionic Phospholipid Inward Translocation and Induces Cholesterol Efflux. *The Journal of biological chemistry* (2013).
27. Robinet, P., Wang, Z., Hazen, S.L. & Smith, J.D. A simple and sensitive enzymatic method for cholesterol quantification in macrophages and foam cells. *Journal of lipid research* **51**, 3364-3369 (2010).
28. Michelsen, K.S. *et al.* Lack of Toll-like receptor 4 or myeloid differentiation factor 88 reduces atherosclerosis and alters plaque phenotype in mice deficient in apolipoprotein E. *Proceedings of the National Academy of Sciences of the United States of America* **101**, 10679-10684 (2004).
29. Ito, A. *et al.* LXRs link metabolism to inflammation through Abca1-dependent regulation of membrane composition and TLR signaling. *eLife* **4**, e08009 (2015).
30. Dong, F., Mo, Z., Eid, W., Courtney, K.C. & Zha, X. Akt inhibition promotes ABCA1-mediated cholesterol efflux to ApoA-I through suppressing mTORC1. *PloS one* **9**, e113789 (2014).
31. Janoudi, A., Shamoun, F.E., Kalavakunta, J.K. & Abela, G.S. Cholesterol crystal induced arterial inflammation and destabilization of atherosclerotic plaque. *European heart journal* **37**, 1959-1967 (2016).
32. Juliana, C. *et al.* Non-transcriptional priming and deubiquitination regulate NLRP3 inflammasome activation. *The Journal of biological chemistry* **287**, 36617-36622 (2012).
33. Ding, J. *et al.* Pore-forming activity and structural autoinhibition of the gasdermin family. *Nature* **535**, 111-116 (2016).
34. Kayagaki, N. *et al.* Caspase-11 cleaves gasdermin D for non-canonical inflammasome signalling. *Nature* **526**, 666-671 (2015).
35. Westerterp, M. *et al.* Deficiency of ATP-Binding Cassette Transporters A1 and G1 in Macrophages Increases Inflammation and Accelerates Atherosclerosis in Mice. *Circulation research* **112**, 1456-1465 (2013).
36. Westerterp, M. *et al.* Cholesterol Accumulation in Dendritic Cells Links the Inflammasome to Acquired Immunity. *Cell metabolism* **25**, 1294-1304 e1296 (2017).
37. Heid, M.E. *et al.* Mitochondrial reactive oxygen species induces NLRP3-dependent lysosomal damage and inflammasome activation. *Journal of immunology* **191**, 5230-5238 (2013).
38. Iyer, S.S. *et al.* Mitochondrial cardiolipin is required for Nlrp3 inflammasome activation. *Immunity* **39**, 311-323 (2013).

39. Dorlo, T.P., Balasegaram, M., Beijnen, J.H. & de Vries, P.J. Miltefosine: a review of its pharmacology and therapeutic efficacy in the treatment of leishmaniasis. *J Antimicrob Chemother* **67**, 2576-2597 (2012).
40. Rios-Marco, P., Marco, C., Cueto, F.J., Carrasco, M.P. & Jimenez-Lopez, J.M. Pleiotropic effects of antitumour alkylphospholipids on cholesterol transport and metabolism. *Exp Cell Res* **340**, 81-90 (2016).
41. Nandi, S. *et al.* ABCA1-mediated cholesterol efflux generates microparticles in addition to HDL through processes governed by membrane rigidity. *Journal of lipid research* **50**, 456-466 (2009).
42. van Hout, G.P. *et al.* The selective NLRP3-inflammasome inhibitor MCC950 reduces infarct size and preserves cardiac function in a pig model of myocardial infarction. *European heart journal* **38**, 828-836 (2017).
43. van der Heijden, T. *et al.* NLRP3 Inflammasome Inhibition by MCC950 Reduces Atherosclerotic Lesion Development in Apolipoprotein E-Deficient Mice-Brief Report. *Arteriosclerosis, thrombosis, and vascular biology* **37**, 1457-1461 (2017).
44. Evavold, C.L. *et al.* The Pore-Forming Protein Gasdermin D Regulates Interleukin-1 Secretion from Living Macrophages. *Immunity* (2017).
45. Chen, J. & Chen, Z.J. PtdIns4P on dispersed trans-Golgi network mediates NLRP3 inflammasome activation. *Nature* (2018).
46. Zhou, R., Tardivel, A., Thorens, B., Choi, I. & Tschopp, J. Thioredoxin-interacting protein links oxidative stress to inflammasome activation. *Nature immunology* **11**, 136-140 (2010).
47. Vaughan, A.M. & Oram, J.F. ABCA1 redistributes membrane cholesterol independent of apolipoprotein interactions. *Journal of lipid research* **44**, 1373-1380 (2003).
48. Wang, S., Gulshan, K., Brubaker, G., Hazen, S.L. & Smith, J.D. ABCA1 mediates unfolding of apolipoprotein AI N terminus on the cell surface before lipidation and release of nascent high-density lipoprotein. *Arteriosclerosis, thrombosis, and vascular biology* **33**, 1197-1205 (2013).

Figure Legends

Figure 1: A) Miltefosine increased ABCA1 mediated cholesterol efflux. RAW264.7 macrophages were labeled with ^{3}H-cholesterol and pretreated with or without 300 μM 8Br-cAMP to induce ABCA1 expression. Cholesterol efflux to chase media was performed for 4h at 37ºC in serum-free DMEM without addition of acceptor containing either vehicle, 7.5 μM or 10 μM Miltefosine. Values are % cholesterol efflux mean ± SD, N=5, different letters above the bars show p<0.01 by ANOVA Bonferroni posttest, with separate analyses for ± ABCA1 induction. ***B)*** Western blot analysis of 8Br-cAMP induced RAW264.7 cell total and cell-surface ABCA1 ± 7.5 μM Miltefosine treatment for 4h. ***C)*** Cholesterol efflux (4h at 37ºC) from ABCA1 stably transfected and control HEK293 to serum-free DMEM without addition of acceptor containing either vehicle, 7.5 μM or 10 μM Miltefosine. Values are % cholesterol efflux mean ± SD, N=3-5, different letters above the bars show p<0.01 by ANOVA Bonferroni posttest, with separate analyses for ± ABCA1 induction. ***D)*** Cholesterol efflux (4h at 37ºC) from ABCA1 and ABCA1 (W590S, C1477R) double mutant (DM) stably transfected HEK293 to serum-free DMEM ± 7.5 μM Miltefosine. Values are % cholesterol efflux mean ± SD, N=3, different letters above the bars show p<0.01 by ANOVA Bonferroni posttest.

Figure 2. ***Miltefosine disrupts lipid-rafts and inhibits PS flip across plasma membrane.*** **A)** GM1 levels assessed by binding of cholera toxin B (CTB) in RAW macrophages ± 7.5 μM Miltefosine for 16h at 37ºC. ***B)*** Flow cytometry quantification of CTB binding of RAW cells treated ± 7.5 μM Miltefosine for 16h at 37ºC. Values are the mean ± SD of the median fluorescence from 3 independent wells (**, p<0.01 by two-tailed t-test). ***C)*** Miltefosine increased cell surface PS. RAW macrophages were incubated with or without 8Br-cAMP to induce ABCA1 and ± 7.5 μM Miltefosine for 16 hrs. PS exposure was determined Annexin V binding via flow cytometry (mean ± SD of the median fluorescence; n = 3 independent wells; *, p<0.05; **, P<0.01; ***, P<0.001 by ANOVA Bonferroni posttest). ***D)*** Miltefosine impairs NBD-PS cellular association with RAW macrophages. Cells were pretreated ± 7.5 μM Miltefosine and incubated with 25 μM NBD-PS at RT for 15 min. ***E)*** Quantification of NBD-PS translocated inside the cells. RAW macrophages were pretreated ± 7.5 μM Miltefosine and incubated with 25 μM NBD-PS at 37ºC for 15 min in phenol red free DMEM. The cells were subjected to flow cytometry analysis in the presence or absence of sodium dithionite to quench extracellular NBD fluorescence, yielding only intracellular NBD fluorescence (mean ± SD % NBD-PS translocated into the cells; N = 3; ***, p<0.001 by two-tailed t-test).

Figure. 3. ***Miltefosine alters plasma membrane PIP2 localization. A***) RAW264.7 cells stably transfected with 2X-PH-PLCeGFP reporter plasmid were treated ± 7.5 μM Miltefosine for 12h at 37ºC. ***B***) RAW264.7 cells stably transfected with 2X-PH-PLCeGFP reporter plasmid were treated ± 7.5 μM Miltefosine for 12h at 37ºC. The cells were fixed, permeabilized, and stained with mouse anti β-actin antibody. ***C)*** Live cell imaging of RAW264.7 cells stably transfected with 2X-PH-PLCeGFP reporter plasmid ± 7.5 μM Miltefosine treatment, stained for β-actin with Phalloidin and DAPI counterstained.

Figure. 4. ***Miltefosine induces autophagy.*** **A)** RAW264.7 cells or LC3-GFP transfected RAW264.7 cells (lower panel) were treated with ± 7.5 μM Miltefosine, followed by staining with p62 antibody (red, upper panel). LC3-GFP protein (green) localization is shown in the lower panel. ***B, C)*** RAW264.7 cells were treated ± 7.5 μM Miltefosine and autophagic flux was assessed in presence of chloroquine for the last 2 h of incubation. The amount of LC3-II was assessed by western blot and densitometry analysis (mean ± SD, N = 3, different letters above the bars represent p<0.001 by ANOVA with Bonferroni posttest). ***D)*** Cellular CE/FC ratio in RAW264.7 cells loaded with 100 μg/ml acetylated low-density lipoprotein (AcLDL) and addition

of 2 µg/ml ACAT inhibitor (ACATi) and/or 7.5 µM Miltefosine as indicated (N=3, mean±SD; *, p<0.05 vs. control; **, p<0.01 vs. control by ANOVA Bonferroni posttest). ***E)*** Lipid droplets assayed by Nile red staining and flow cytometry ± AcLDL loading, ± 4 hr chase ± 7.5 µM Miltefosine and/or 2 µg/ml ACATi, as indicated (mean ± SD, N = 3, different letters above the bars represent p<0.05 by ANOVA with Bonferroni posttest).

Figure. 5. Miltefosine dampened TLR4 signaling in bone marrow derived macrophages. A) Mouse BMDMs were treated with ± 5 µM Miltefosine for 16h at 37ºC and primed by incubation with ± 1mg/ml LPS at 37ºC for 4hrs, followed by mRNA preparation and qRT-PCR analysis of pro-IL-1β transcript with actin used as control transcript (N=6, mean ± SD; different letters above the bars represent p<0.01 by ANOVA with Bonferroni posttest). ***B)*** Mouse BMDMs were treated with ± 5 µM Miltefosine and primed by incubation with ± 1mg/ml LPS followed by western blot analysis using IL1-β antibody. GAPDH was used as loading control.

Figure. 6. Miltefosine inhibited Nlrp3 inflammasome assembly and IL-1β release. A) Mouse BMDMs were pretreated with ± 5 µM Miltefosine, primed by incubation with ± 1µg/ml LPS, and induced for Nlrp3 inflammasome assembly by incubation with 1 mM ATP for 20 min. Cells were fixed and stained with anti-ASC with DAPI counterstaining. ***B)*** Released IL-1β levels in media was reduced by 5 µM Miltefosine pretreatment from cells treated with LPS and ATP. ***C)*** qRT-PCR analysis of NLRP3, GsdmD and caspase 1 mRNAs, relative to β-actin mRNA, from mouse BMDMs ± 5 µM Miltefosine pretreatment, ± LPS treatment (N=6, mean ± SD; different letters represent p<0.05 by ANOVA with Bonferroni posttest). ***D)*** IL-1β released from mouse BMDMs treated with ± 5 µM Miltefosine and primed with 1µg/ml LPS, followed by transfection with 2µg of poly (dA-dT) for 3h to induce the AIM2 inflammasome. ***E)*** Total cholesterol levels were determined in mouse BMDMs treated with ± 5 µM Miltefosine for 16h or 1 mM cyclodextrin for 2h. ***F)*** IL-1β released from mouse BMDMs treated ± 5 µM Miltefosine for 16h or 1 mM cyclodextrin for 2h followed by LPS and ATP treatment (mean ± SD, N = 3, different letters above the bars represent p<0.05 by ANOVA with Bonferroni posttest).

Figure. 7*. Miltefosine alters mitochondrial homeostasis.** ***A) Miltefosine decreases mitochondrial ROS, shown by live cell imaging of mitochondrial ROS detected by MitoSox staining of mouse BMDMs pretreated ± 5 µM Miltefosine and treated ± 1µg/ml LPS. ***B)*** Flow-cytometry analysis showing quantification of MitoSox staining of BMDMs treated as indicated (mean ± SD, N = 3, different letters above the bars represent p<0.01 by ANOVA with Bonferroni posttest). ***C)*** Live cell flow cytometry of mitochondrial membrane potential detected by TMRM staining of mouse BMDMs pretreated ± 5 µM Miltefosine and treated ± 1µg/ml LPS (mean ± SD, N = 3, different letters above the bars represent p<0.05 by ANOVA with Bonferroni posttest). ***D)*** Miltefosine induces mitophagy shown by live cell imaging of RAW264.7 cells treated ± 7.5 µM Miltefosine using the Mitophagy Detection kit.

Figure 1

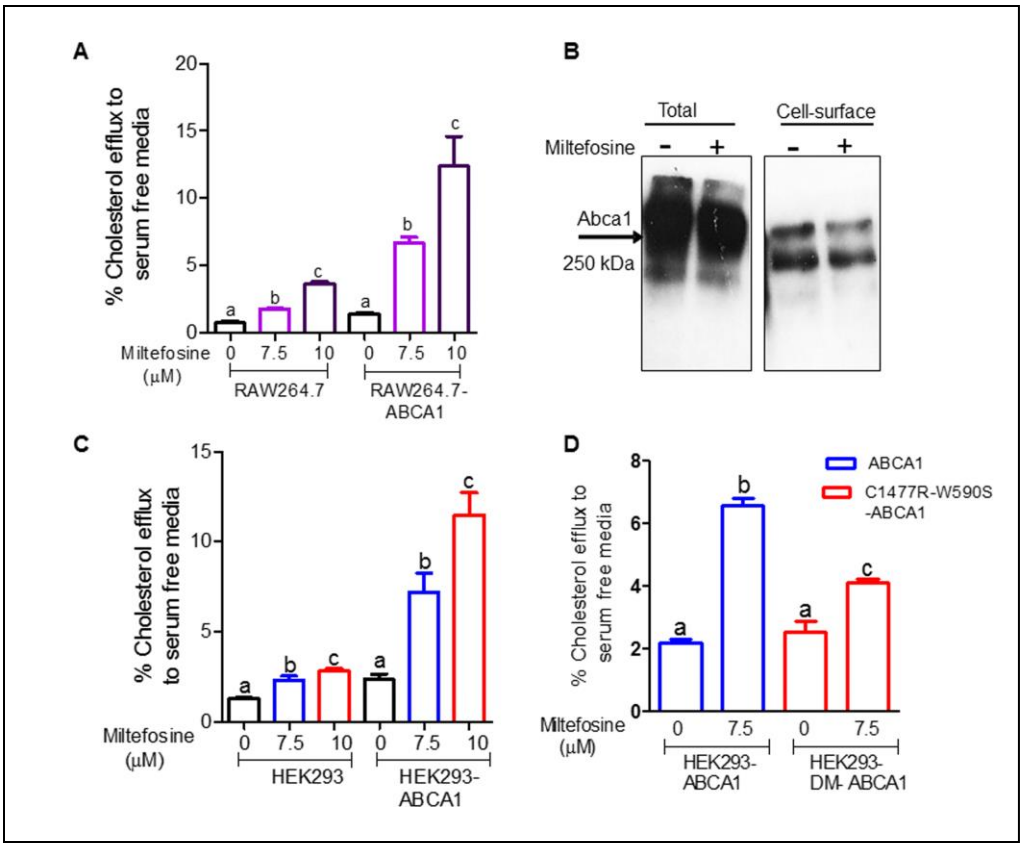
A
% Cholesterol efflux to serum free media
20
15
10
5
0
a
b
c
a
b
c
Miltefosine (μM)
0
7.5
10
0
7.5
10
RAW264.7
RAW264.7-ABCA1
B
Total
Cell-surface
Miltefosine
-
+
-
+
Abca1
250 kDa
C
% Cholesterol efflux to serum free media
15
10
5
0
a
b
c
a
b
c
Miltefosine (μM)
0
7.5
10
0
7.5
10
HEK293
HEK293-ABCA1
D
% Cholesterol efflux to serum free media
8
6
4
2
0
ABCA1
C1477R-W590S -ABCA1
a
b
a
c
Miltefosine (μM)
0
7.5
0
7.5
HEK293-ABCA1
HEK293-DM- ABCA1

Figure 2

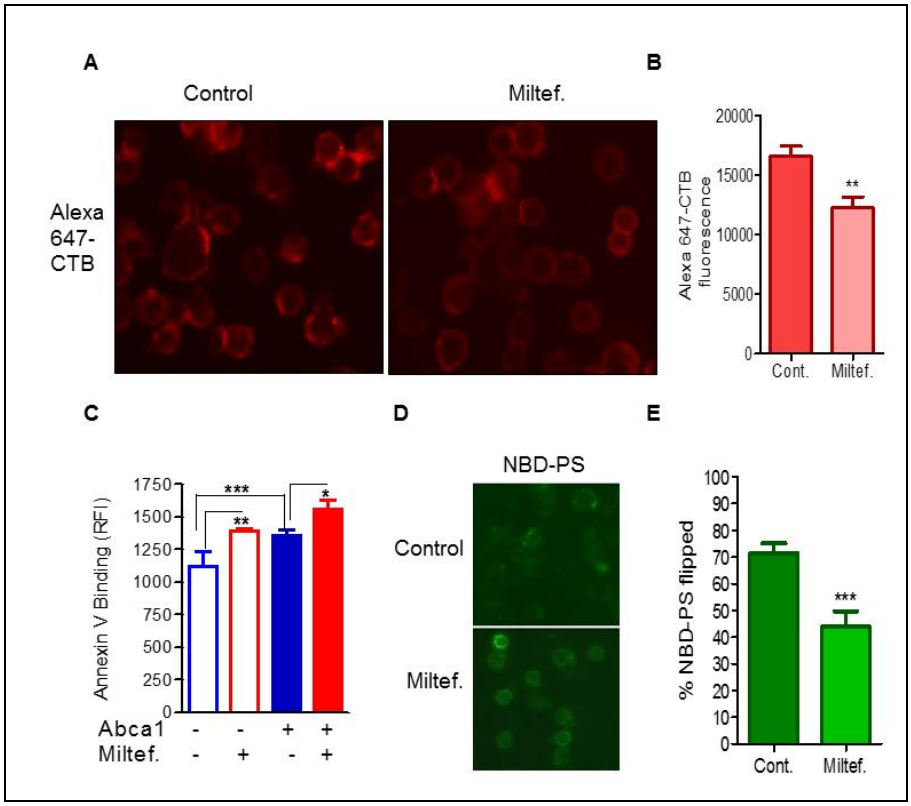
A
Control
Miltef.
Alexa 647-CTB
B
Alexa 647-CTB fluorescence
20000
15000
10000
5000
0
**
Cont.
Miltef.
C
Annexin V Binding (RFI)
1750
1500
1250
1000
750
500
250
0
***
**
*
Abca1 - - + +
Miltef. - + - +
D
NBD-PS
Control
Miltef.
E
% NBD-PS flipped
100
90
80
70
60
50
40
30
20
10
0
***
Cont.
Miltef.

Figure 3

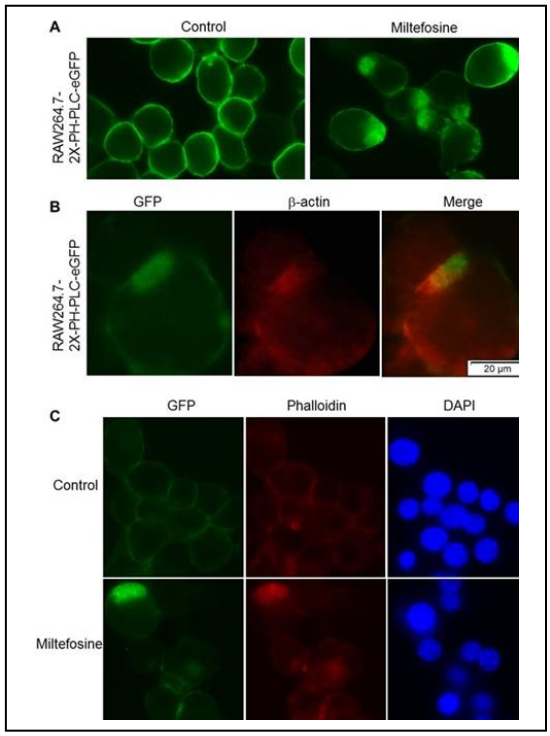
A
Control
Miltefosine
RAW264.7-
2X-PH-PLC-eGFP
B
GFP
β-actin
Merge
RAW264.7-
2X-PH-PLC-eGFP
20 μm
C
GFP
Phalloidin
DAPI
Control
Miltefosine

Figure 4

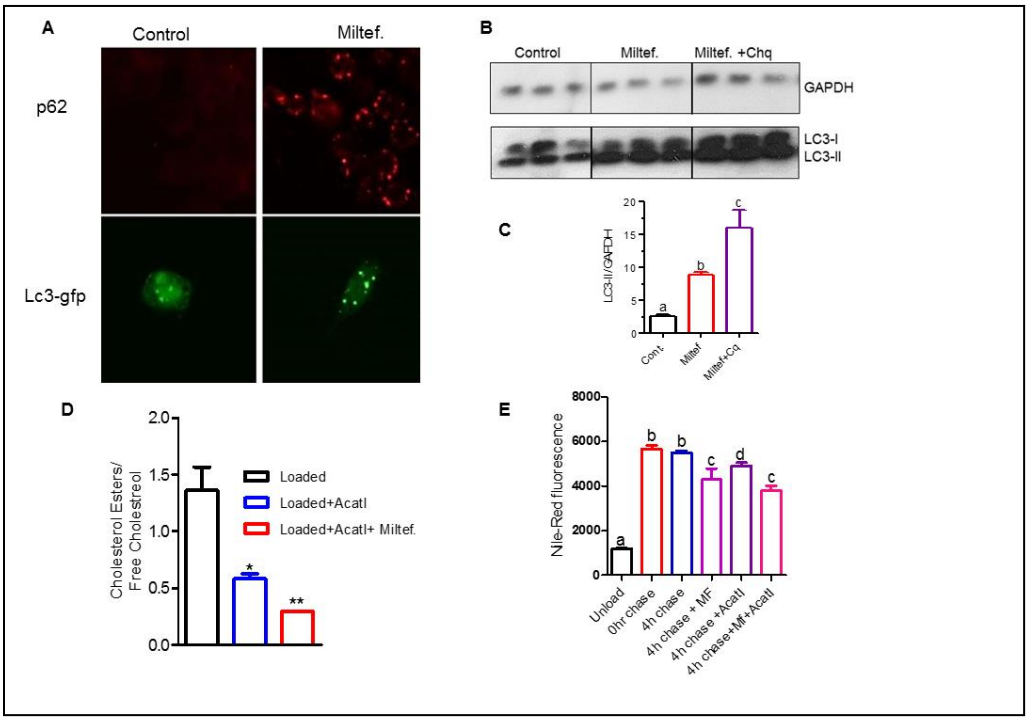
A
Control
Miltef.
p62
Lc3-gfp
B
Control
Miltef.
Miltef. +Chq
GAPDH
LC3-I
LC3-II
C
LC3-II/GAPDH
Cont.
Miltef
Miltef+Cq
D
Cholesterol Esters/
Free Cholestreol
Loaded
Loaded+Acatl
Loaded+Acatl+ Miltef.
E
Nile-Red fluorescence
Unload
0hr chase
4h chase
4h chase + MF
4h chase +Acatl
4h chase+Mf+Acatl

Figure 5

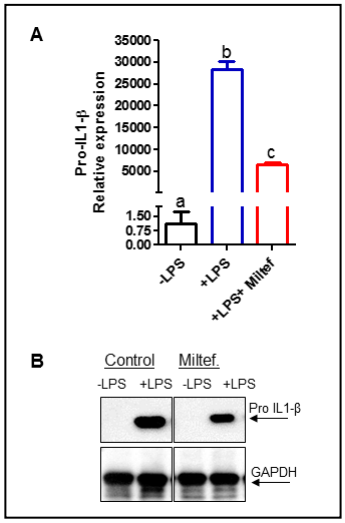
A
Pro-IL1-β
Relative expression
35000
30000
25000
20000
15000
10000
5000
1.50
0.75
0.00
a
b
c
-LPS
+LPS
+LPS+ Miltef
B
Control
Miltef.
-LPS
+LPS
-LPS
+LPS
Pro IL1-β
GAPDH

Figure 6

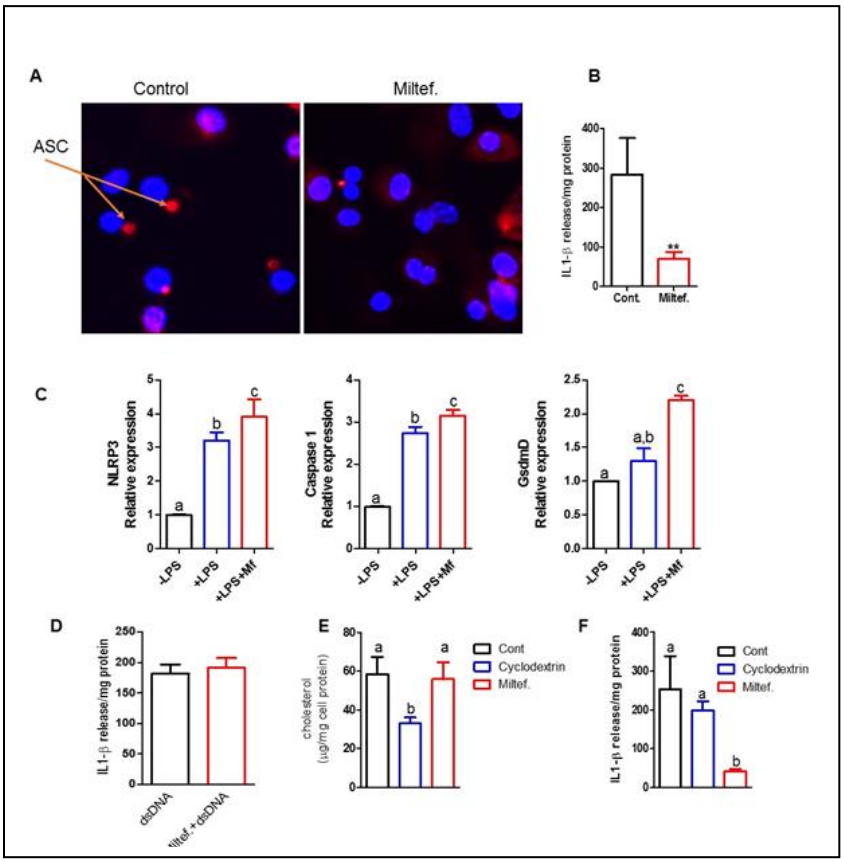
A
Control
Miltef.
ASC
B
IL1-β release/mg protein
400
300
200
100
0
**
Cont.
Miltef.
C
NLRP3
Relative expression
Caspase 1
Relative expression
GsdmD
Relative expression
-LPS
+LPS
+LPS+Mf
D
IL1-β release/mg protein
dsDNA
Miltef.+dsDNA
E
cholesterol
(µg/mg cell protein)
Cont
Cyclodextrin
Miltef.
F
IL1-β release/mg protein
Cont
Cyclodextrin
Miltef.

Figure 7

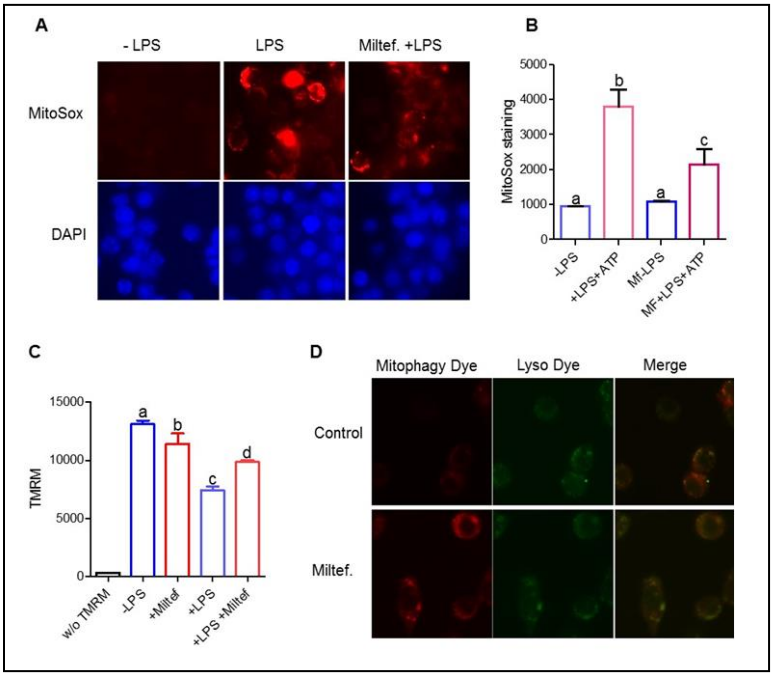
A
- LPS
LPS
Miltef. +LPS
MitoSox
DAPI
B
MitoSox staining
5000
4000
3000
2000
1000
0
a
b
a
c
-LPS
+LPS+ATP
MF-LPS
MF+LPS+ATP
C
TMRM
15000
10000
5000
0
a
b
c
d
w/o TMRM
-LPS
+Miltef
+LPS
+LPS +Miltef
D
Mitophagy Dye
Lyso Dye
Merge
Control
Miltef.

SI Materials and Methods.

Materials: The RAW264.7 cells were from ATCC. Miltefosine and 18:1 NBD-PS were obtained from Avanti polar and methyl-β-cyclodextrin is obtained from Sigma Aldrich. ^{3}H-cholestreol (NET13900) was obtained from Perkin- Elmer. Antibodies were purchased from various sources (see table below). MitoSox reagent, Image-iT ™ TMRM reagent, and Alexa FluorTM555 Phalloidin were purchased from Invitrogen.

NovusBio	ABCA1	NB400-05
Cell signaling:	GAPDH (14C10) Rabbit mAb	2118
	NLRP3 (D4D8T) Rabbit mAb	15101
	PIKBa (Ser32) (14D4) Rabbit mAb	2859
	NF-κB p65 (C22B4) Rabbit mAb	4764
	Phospho-AmpKa (The172) (40H9) Rabbit mAb	2535S
	AmpKa Ab	2532S
	Phospho-ULK1 (Ser757) (D7O6U) Rabbit mAb	14202T
	ULK1 (D8H5) Rabbit mAb	8054T
	Albumin Antibody	#4929
Abclonal	GSDMD	A10164
Invitrogen	Pip4k2a	PA5-31141
Abcam	Nek7	Ab133514

Isolation of Bone marrow derived macrophages: All experiments were performed in accordance with protocols approved by the Cleveland Clinic Institutional Animal Care and Use Committee (ICUC). WT C57BL/6 or C57BL/6 *ApoE*$^{-/-}$ mice were maintained on chow diet and sacrificed at 16 weeks of age. Femurs were collected to isolate and culture bone marrow macrophages using conditioned L-cell media. Mice were euthanized by CO_2 inhalation and femoral bones were removed. The marrow was flushed out of the bones into a 50 ml sterile tube using a 10 ml syringe with a 26 gauge

needle filled with sterile DMEM. Cells were centrifuged for 5 min at 1,800 rpm at 4°C, followed by two washes with sterile PBS. The cells were resuspended in sterile-filtered BMDM growth media (DMEM with 7.6% fetal bovine serum, 15% L-cell conditioned media, and 0.76% penicillin/streptomycin mixture) and plated in 10 cm culture dishes and incubated at 37°C for 14 days. Cell media was replaced every 2–3 days for 2 weeks. The cells were routinely visualized under microscope for proliferation and differentiation into confluent BMDMs.

Isolation of total RNA from BMDM cell pellets and RT-PCR analysis: Total RNA was isolated from the cell pellets using RNeasy Mini Kit (Qiagen Inc. Valencia, CA). One µg of total RNA was reverse transcribed using the iScript cDNA kit (Biorad). Real-time PCR amplification was performed using TaqMan and gene-specific primers in a StepOnePlus™ real time PCR machine (Applied Biosystems) in triplicate. The relative amount of target mRNA was determined using the cycle threshold (Ct) method by normalizing target mRNA Ct values to that of β-actin. The Fold induction ratios were calculated relative to control sample for each group using the formula $2^{-\Delta\Delta Ct}$.

The reagents were obtained from Qiagen, Biorad, and ThermoFisher (see table below).

Qiagen	RNEasy MiniKit	74104
Qiagen	Rnase-free Dnase set	79254
Biorad	iScript cDNA kit	170-8891
ThermoFisher	2x TaqMan	4304437
ThermoFisher	NIrp3	Mm00840904
	Casp1	Mm00438023
	Pycard	Mm00445747
	iL1B	Mm00434228
	Gsdmd	Mm00509958
	Actb	Mm02619580

Cholesterol efflux assay: The cholesterol efflux assays were performed in HEK293-Abca1-GFP cells, BHK cells, or RAW 264.7 murine macrophages. The cells were plated

in 24-well plates at a density of 300-400,000 cells per well. The cells were labeled with ^{3}H cholesterol in 1% FBS in DMEM for 24h. The labeled cells were induced for ABCA1 expression for 16h with 0.3 mM 8Br-cAMP (for RAW264.7 cells) or with 10nM Mifepristone (for BHK cells). Inducers were included in the media during subsequent assays. ABCA1 expression was confirmed by western blot using the AC10 antibody. The cells were washed with serum free media and chased for indicated time period in serum-free DMEM in the presence or absence of indicated treatments. The radioactivity in the chase media was determined after brief centrifugation to pellet any residual debris. Radioactivity in the cells was determined by extraction in hexane:isopropanol (3:2) with the solvent evaporated in a scintillation vial prior to counting. The percent cholesterol efflux was calculated as 100 × (medium dpm) / (medium dpm + cell dpm).

Lipid-Raft quantification: The lipid-raft were visualized under fluorescent microscope and quantified using flow-cytometry assay. RAW cells were treated with 7.5 µg/ml Miltefosine at 37ºC for 16h. For imaging, cells were treated with 1 µg/ml Alexa647-CT-B labeled cells and images were captured using epifluorescent microscopy. For quantification, the cells were washed twice with PBS and gently scraped in 1.5 ml PBS. The Alexa647-CT-B (1µl of 1.5 mg/ml stock in PBS was added to 1.5 ml cells) was added at final concentration of 1 µg/ml to cells in 5 ml polystyrene round-bottom tubes (12 X 75 mm). The samples were subjected to Flow analysis with BD Biosciences LSRII cytometer using laser (Alexa 647 (Red) Ex: 639, Em: 650-670, Filter 660/20) and data was analyzed by Flowjo software.

Cell-surface PS and NBD-PS translocation: To measure cell surface PS, cells were cultured in 6 well plates in growth media, washed twice with PBS, and were resuspended in 500 µl Annexin V binding buffer plus 1 µl of Annexin V-Cy5 (Biovision). The samples were incubated at room temperature for 5 minutes in the dark. Flow cytometry analysis was performed using a BD Biosciences LSRFortessa cytometer using a 639 nm excitation laser and emission at 650-670 nm; and, data was analyzed using Flowjo software. To measure the inward translocation of various NBD labeled PS, RAW cells were incubated with phenol-red free DMEM containing 25 µM NBD-PS for 15 min at RT. The media was then replaced with PBS. The cells were gently scraped and were subjected to flow cytometry analysis first without sodium dithionite to calculate total NBD fluorescence, and then 5 min after the addition of 30 µl of a freshly prepared 1M sodium dithionite solution to determine the fraction of the signal resistant to quenching (translocated signal). Flow cytometry analysis was performed as above using a 488 nm laser for excitation and emission at 505-525 nm.

Western blotting: RAW264.7 cells or BMDMs were grown treated as indicated. The PBS-washed cell pellet was lysed in NP40 lysis or MPER lysis buffer. After discarding the nuclear pellet, the protein concentration was determined using the BCA protein assay (Pierce). 10-50 µg of cell protein samples were resolved on Novex 4-20% Tris-Glycine Gels (Invitrogen) and transferred onto polyvinylidene fluoride membranes (Invitrogen). Blots were incubated sequentially with 1:1000 rabbit polyclonal antibody raised against Nlrp3 (cell signaling), or 1:5000 rabbit polyclonal antibody raised against P-AMPK (cell signaling), or 1:1000 rabbit polyclonal antibody raised against IL1-b (cell signaling), 1:1000 rabbit polyclonal antibody raised against Gasdermin D, 1:1000 rabbit

polyclonal antibody raised against ASC1. The signal was detected with an enhanced chemiluminescent substrate (Pierce). For LC3 western blot, RAW264.7 cells were incubated with or without 7.5 μM Miltefosine for 16 h, indicated wells received 30 μM chloroquine during the last 2 h of incubation. Blots were sequentially incubated with 1:1,000 rabbit polyclonal antibody raised against LC3B and 1:10,000 horseradish peroxidase-conjugated goat anti-rabbit as described above. GAPDH was used as a loading control.

Total and cell surface ABCA1 levels: RAW 267.4 cells were cultured in DMEM with 10% FBS and were treated with 300 μM 8Br-cAMP to induce ABCA1 for 16 hr. Cells were incubated with incubated with or without 7.5μM Miltefosine for 4h. The cells were then incubated for 30 minutes on ice with phosphate-buffered saline (PBS) containing 1 mg/mL sulfo-NHS-biotin (Pierce). The PBS-washed cell pellet was lysed in 200 μl of lysis buffer (150 mM sodium chloride, 5 mM EDTA, 50 mM Tris-phosphate pH 8.0, 1% NP40, and 10% protease inhibitor). Cell-surface ABCA1 was determined by purifying biotinylated proteins by overnight incubation of 250 ug of cell protein with 75 uL of UltraLink Plus Immobilized Streptavidin gel (Pierce) at 4°C. The beads were spun down, washed, and resuspended by boiling in 100 μl 1x NuPage LDS Sample buffer (Invitrogen) and 20 μg of total protein were run on NuPAGE 3-8% Tris-Acetate gels (Invitrogen) and transferred onto polyvinylidene fluoride membranes (Invitrogen). Blots were incubated sequentially with 1:500 mouse monoclonal antibody raised against ABCA1 (AC10) and 1:15 000 horseradish peroxidase-conjugated goat anti-mouse secondary antibody (Biorad). The signal was detected with an enhanced chemiluminescent substrate (Pierce).

Supplementary Figure Legends

Figure S1: Miltefosine increased ABCA1 mediated cholesterol efflux. BHK cells were labeled with ^{3}H-cholesterol and pretreated with or without Mifepristone to induce ABCA1 expression. Cholesterol efflux to chase media was performed for 4h at 37°C in serum-free DMEM without addition of acceptor containing either vehicle, 7.5 μM or 10 μM Miltefosine. Values are % cholesterol efflux mean ± SD, N=5, different letters above the bars show $p<0.01$ by ANOVA Bonferroni posttest, with separate analyses for ± ABCA1 induction.

Figure S2: Miltefosine increased microparticle generation. RAW cells were treated with ± 7.5 μM Miltefosine for 4h at 37°C. The media was collected and cleared of cell debris by centrifugation at 5K rpm for 5 min. The supernatant was spun down at 15K for 30 min. The pellet was suspended in sterile PBS (filtered with 0.22 μM filter) and microparticle were detected using Zetaview particle analyzer. Values are number of microparticles per ml, mean ± SD, N=3, different letters above the bars show $p<0.001$ by t-test.

Figure S3: Miltefosine decreased lipid droplets. RAW cells were loaded with 100μg/ml AcLDL for 24h, followed by 4 hr chase ± 7.5 μM Miltefosine for 4h at 37°C. The cells were then stained with Nile-red and counterstained with DAPI and imaged using fluorescent microscope.

Figure S4: Miltefosine induced AMPK phosphorylation. RAW cells were treated ± 7.5 μM Miltefosine for 4h at 37°C. The cells extracts were prepared in MPER lysis buffer containing phosSTOP (Roche). Western blot analysis was carried out using anti-Phosho-AMPK and AMPK antibodies.

Figure S5: Miltefosine inhibited Nlrp3 inflammasome assembly. Full image of cropped section shown in ***Figure 6A***. Asc specks and DAPI staining in control BMDMs.

Figure S6: Miltefosine inhibited Nlrp3 inflammasome assembly. Full image of cropped section shown in ***Figure 6A***. Asc specks and DAPI staining in Miltefosine treated BMDMs.

Figure S7: Miltefosine did not alter the protein levels of Nlrp3 inflammasome complex. Mouse BMDMs were treated with ± 5 μM Miltefosine for 16h at 37°C. The cells were primed by incubation with ± 1mg/ml LPS at 37°C for 4hrs, followed by cell extract preparation and western blot analysis using NLRP3 antibody (***A***), ASC (***B***), Caspase 1 (***C***) and Gasdermin D (***D***). GAPDH was used as loading control.

Figure S8: Miltefosine inhibited Nlrp3 inflammasome assembly. Asc specks and DAPI staining in cyclodextrin treated BMDMs.

Figure S9: Miltefosine altered mitochondrial homeostasis. TMRM staining of mouse BMDMs pretreated ± 5 μM Miltefosine and treated ± 1μg/ml LPS.

Figure S10: Miltefosine altered mitochondrial homeostasis. Mouse BMDMs pretreated ± 5 µM Miltefosine were stained with mitophagy dye (Mitophagy detection kit MD01, Dojindo Molecular Technologies, Inc.)

Figure S1, S2

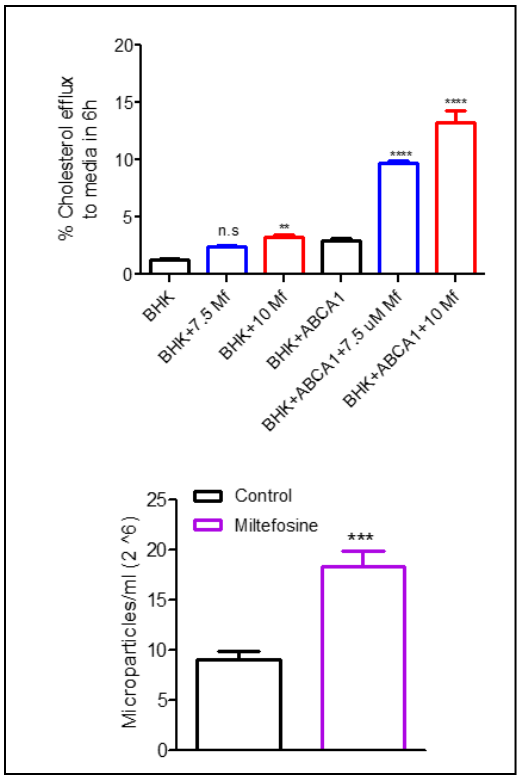
% Cholesterol efflux to media in 6h
20
15
10
5
0
n.s
**
****
****
BHK
BHK+7.5 Mf
BHK+10 Mf
BHK+ABCA1
BHK+ABCA1+7.5 uM Mf
BHK+ABCA1+10 Mf
Microparticles/ml (2 ^6)
25
20
15
10
5
0
Control
Miltefosine
***

Figure S3, S4

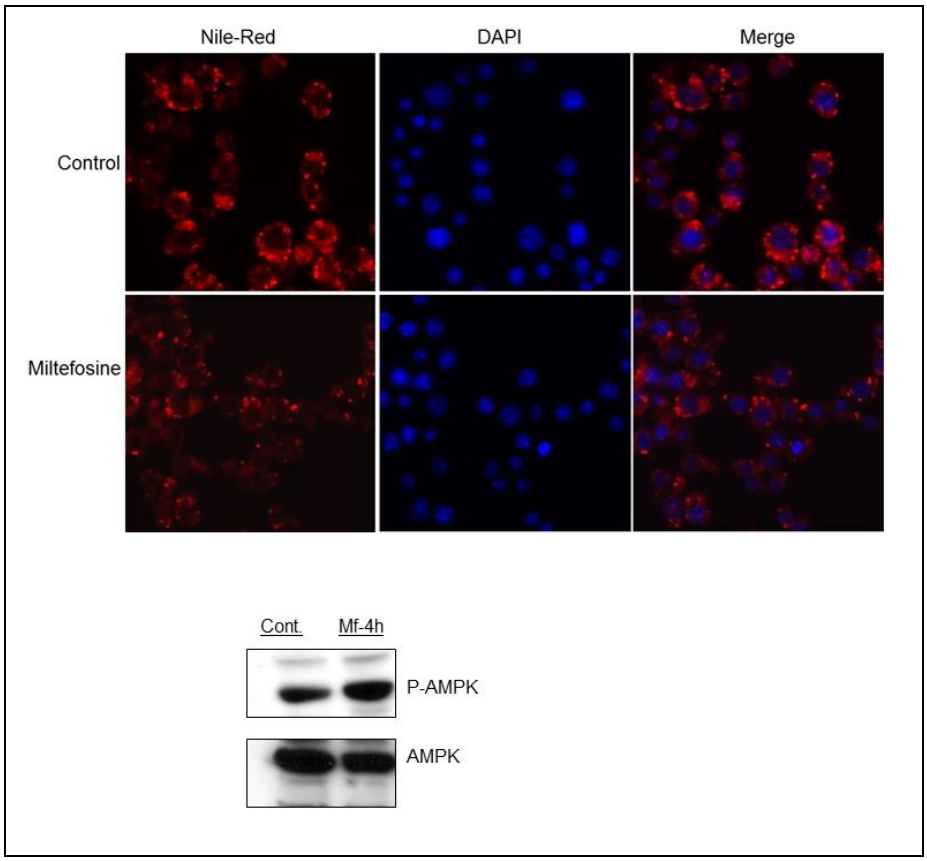
Nile-Red
DAPI
Merge
Control
Miltefosine
Cont.
Mf-4h
P-AMPK
AMPK

Fig. S5

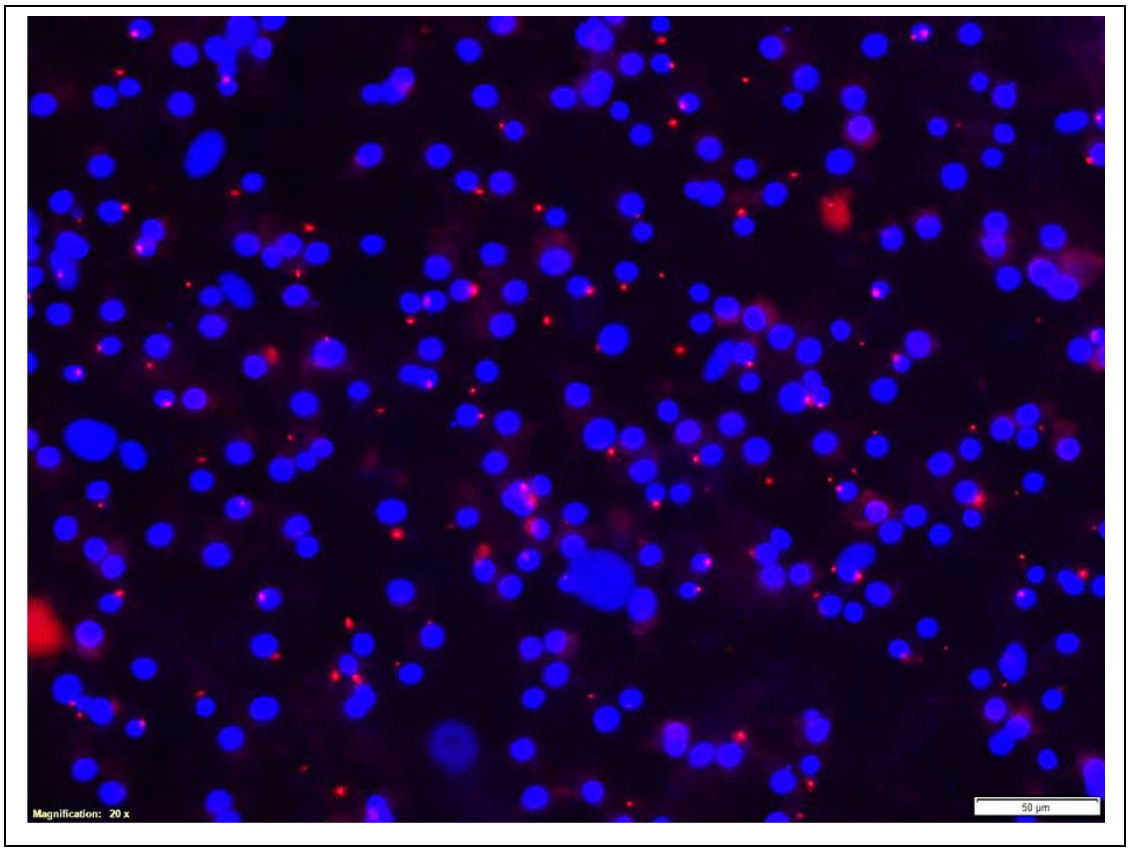

Fig. S6

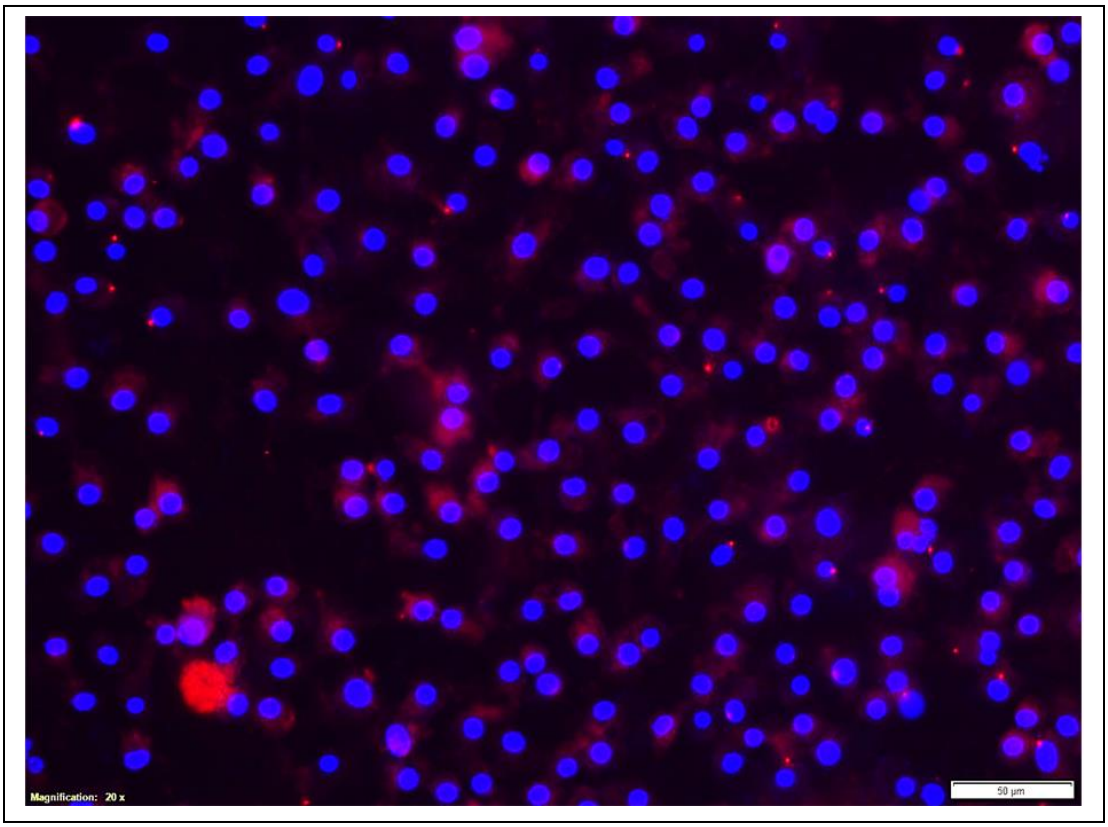

Fig. S7

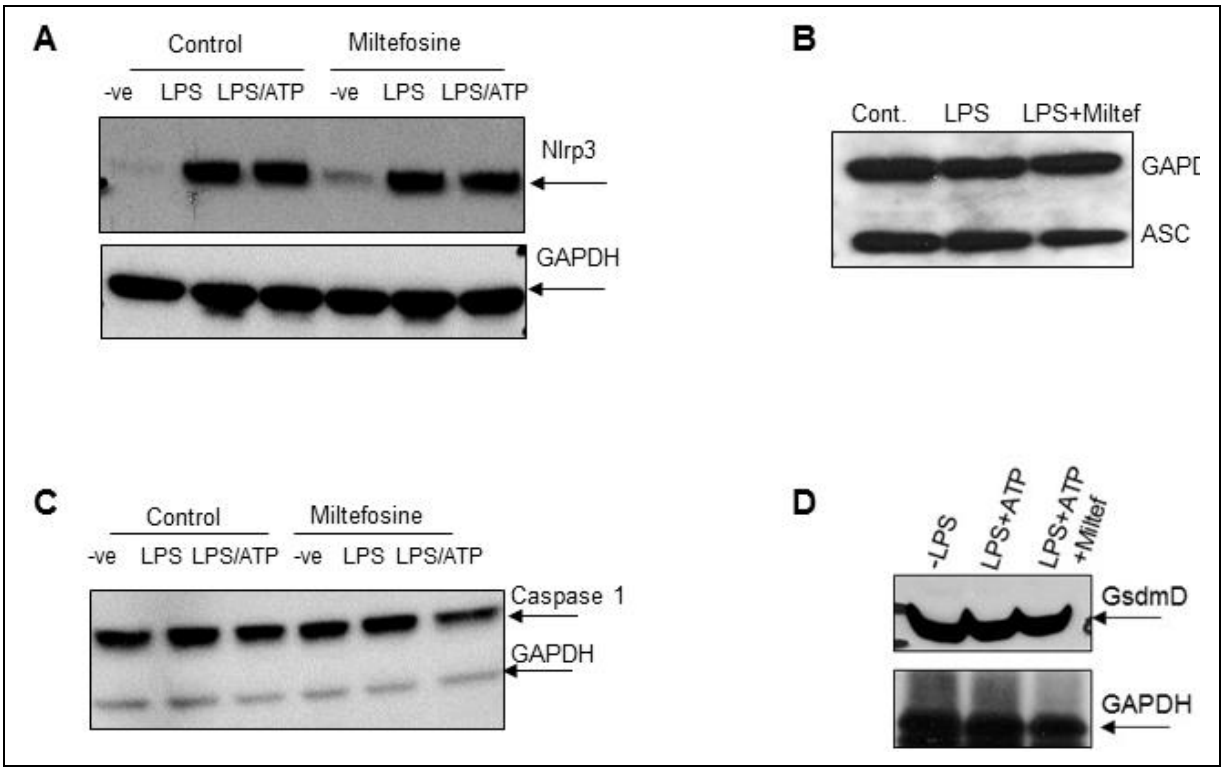
A
Control
Miltefosine
-ve
LPS
LPS/ATP
-ve
LPS
LPS/ATP
Nlrp3
GAPDH
B
Cont.
LPS
LPS+Miltef
GAPD
ASC
C
Control
Miltefosine
-ve
LPS
LPS/ATP
-ve
LPS
LPS/ATP
Caspase 1
GAPDH
D
-LPS
LPS+ATP
LPS+ATP +Miltef
GsdmD
GAPDH

Fig. S8

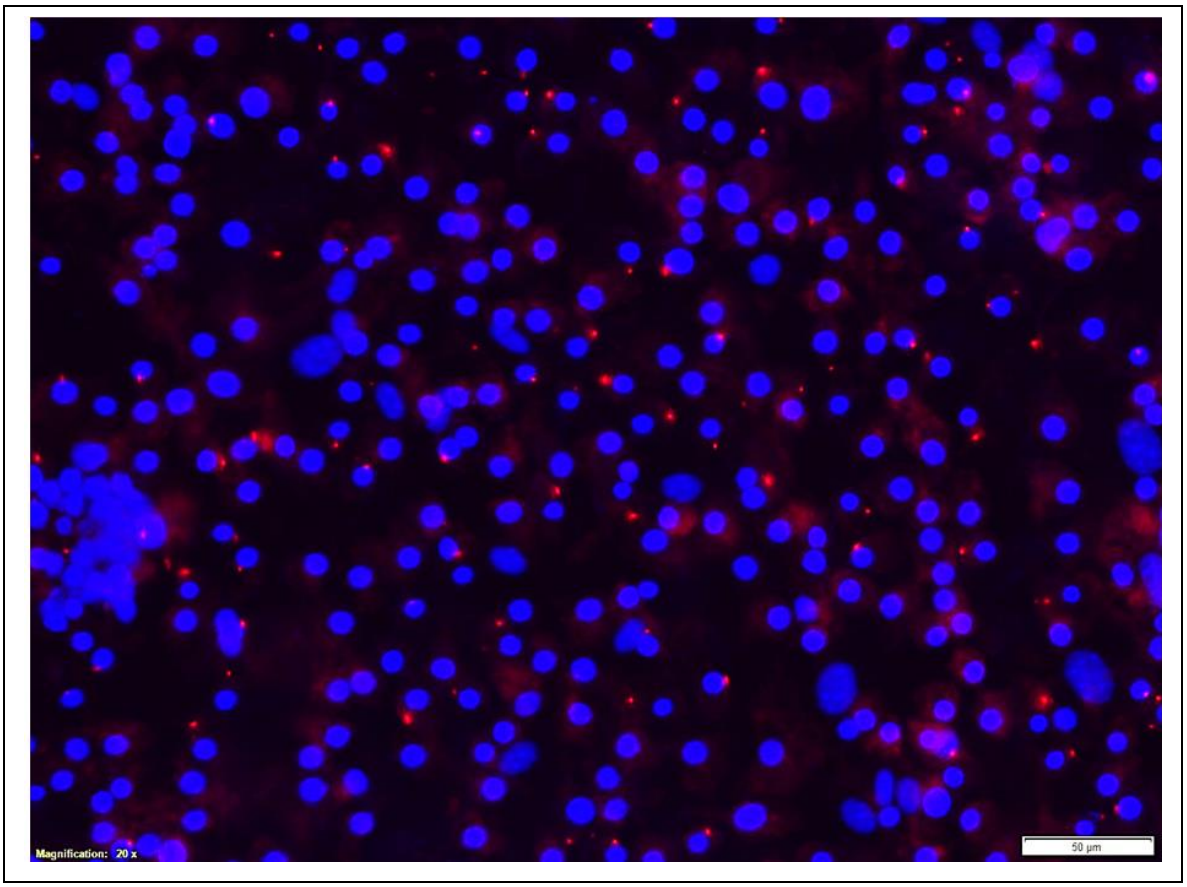

Fig. S9

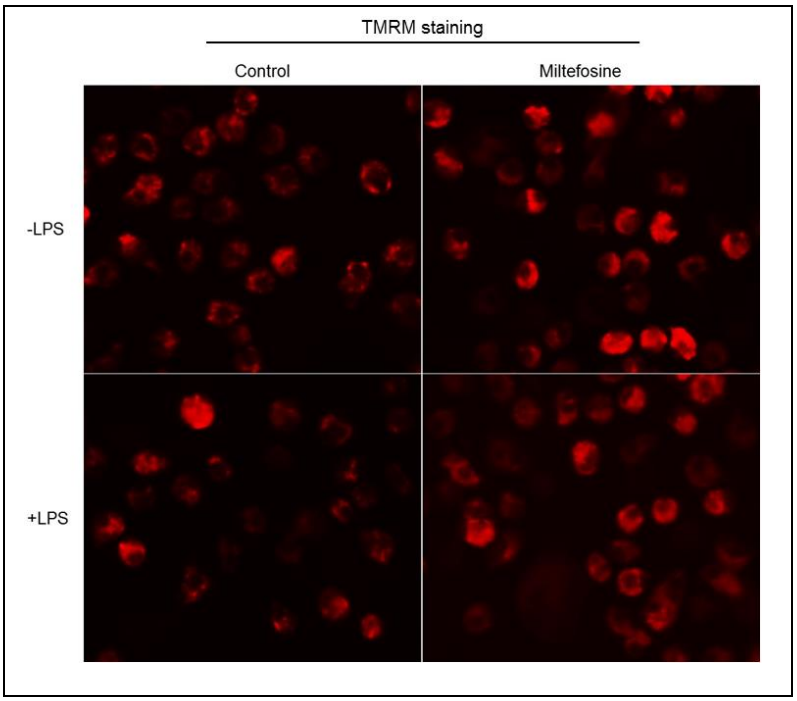
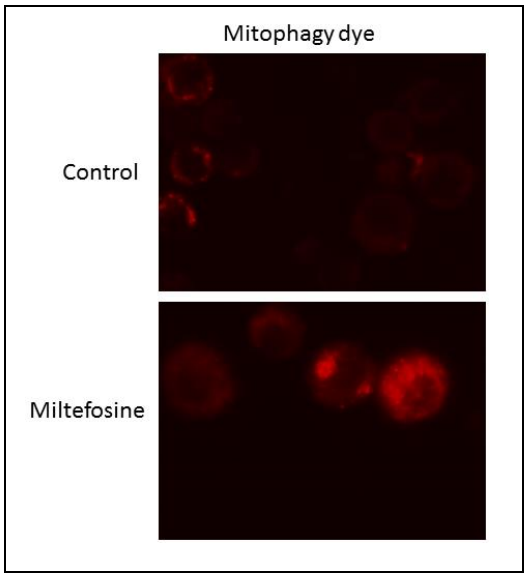
Fig. S10